Available online at www.sciencedirect.com

ScienceDirect

IFAC Papers Online CONFERENCE PAPER ARCHIVE

IFAC PapersOnLine 59-20 (2025) 333–338

Model-free adaptive multivariable control of nonlinear twin-rotor dynamics in the presence of wind gust: A comparison of different approaches

Hasan Abbasi Nozari * **Shahrzad Hedayati** **
Paolo Castaldi *** **Jalil Sadati Rostami** *

* *Faculty of Electrical and Computer Engineering, Babol Noshirvani University of Technology, Babol, Iran.*
** *Department of Biomedical Engineering,Rouzbahan Institute of Higher Education, Sari, Iran.*
*** *Department of Electrical, Electronic and Information Engineering, University of Bologna, Via Dell'Università 50, 47521, Cesena, Italy*

Abstract: This study proposes a data-driven model-free adaptive controller (DDMFAC) for a Multi Input-Multi Output (MIMO) twin-rotor aerodynamic system. The primary objective is to achieve precise beam tracking and accurate positioning in two degrees of freedom (DOF) for azimuth and pitch control. To this end, Three MFAC algorithms—Compact Form Dynamic Linearization (CFDL), Partial Form Dynamic Linearization (PFDL), and Full Form Dynamic Linearization (FFDL)—are employed for azimuth and pitch tracking, evaluated under both wind-free and windy conditions. A comparative analysis showcases the performance and tracking capabilities of these three model-free methods and their efficacy in controlling the MIMO twin-rotor system under various conditions. Additionally, the adaptive laws are designed to enhance robustness against wind gusts, ensuring reliable control under external disturbances.

Copyright © 2025 The Authors. This is an open access article under the CC BY-NC-ND license (https://creativecommons.org/licenses/by-nc-nd/4.0/)

Keywords: Data-driven control, twin Rotor dynamics, model free adaptive control, pseudo partial derivative, dynamic linearization data model.

1. INTRODUCTION

The Twin Rotor Multi-Input Multi-Output System (TRMS) is a widely-used tool for studying and designing control strategies for two degrees of freedom helicopters and multi-rotor systems within a controlled laboratory environment. These systems serve as simplified models due to their structural design, which incorporates two perpendicular rotors mounted on a shared beam CANKURT (2018). The TRMS is an aerodynamic system that exhibits complex nonlinear behavior and significant coupling effects between its two propellers [1]. In contrast to a typical helicopter, where the aerodynamic force is controlled by adjusting the angle of attack of the propeller blades (Sandino et al. (2013), Godbolt et al. (2013)), the TRMS features a fixed blade angle. Instead, the aerodynamic force is managed by altering the speed of the motors Wen and Lu (2008). This setup enables the study of various control approaches for nonlinear MIMO systems. The main beam, which connects the rotors, is capable of both horizontal and vertical rotation while being pivoted from the base. An additional beam, placed perpendicular to the main beam between the rotors, can be utilized for attaching counterweights to the system CANKURT (2018). Over the years, various control strategies have been developed and implemented to effectively control the TRMS, ranging from classical to advanced and intelligent techniques [Rahideh et al. (2007), Rahideh et al. (2012), Tao et al. (2010), Juang et al. (2008a), Roman et al. (2017), Roman et al. (2015), Juang et al. (2008b)]. These efforts have contributed to enhancing our understanding and control of such complex aerodynamic systems.

2. MODELING OF TWIN ROTOR MIMO SYSTEM

TRMS is composed of two rotors: a main rotor and a tail rotor. Thrust is generated as a result of the rotor moving a mass of air in front of it, causing the rotor to experience a counteracting force known as thrust, in accordance with the laws of conservation. The TRMS model is designed for compatibility with the Simulink environment. The DC motor with a propeller is modeled as a linear dynamic system, followed by a static nonlinear component. The vertical movement's momentum equation can be expressed as follows:

$$I_1 \cdot \ddot{\alpha}_v = M_1 - M_{FG} - M_{B\alpha_v} - M_G, \qquad (1)$$

2405-8963 Copyright © 2025 The Authors. This is an open access article under the CC BY-NC-ND license.
Peer review under responsibility of International Federation of Automatic Control.
10.1016/j.ifacol.2025.11.172

where the nonlinear static characteristic can be described as:

$$M_1 = a_1 \cdot \tau_1^2 + b_1 \cdot \tau_1. \tag{2}$$

The gravity momentum can be expressed as:

$$M_{FG} = M_g \cdot \sin \alpha_v. \tag{3}$$

The friction forces momentum is described as:

$$M_{B\alpha_v} = B_{1\alpha_v} \cdot \dot{\alpha}_v - \frac{0.0326}{2} \sin 2\alpha_v \cdot \dot{\alpha}_h^2. \tag{4}$$

The gyroscopic momentum is given by

$$M_G = k_{gy} \cdot M_1 \cdot \dot{\alpha}_h \cdot \cos \alpha_v. \tag{5}$$

In the Laplace domain, the main DC motor momentum is modeled using a first-order transfer function. This approximation simplifies the representation of the motor and its associated electrical control circuit. The transfer function is given by

$$\tau_1 = \frac{k_1}{T_{11}s + T_{10}} \cdot u_1. \tag{6}$$

The momentum equation for the horizontal movement can be written as:

$$I_2 \cdot \ddot{\alpha}_h = M_2 - M_{B\alpha_h} - M_R, \tag{7}$$

where the nonlinear static characteristic is given by

$$M_2 = a_2.\tau_2^2 + b_2.\tau_2. \tag{8}$$

The friction forces momentum is represented as:

$$M_{B\alpha_h} = B_{1\alpha_h} \cdot \dot{\alpha}_h, \tag{9}$$

and cross-reaction momentum, M_R, is expressed as:

$$M_R = \frac{k_c\,(T_o s + 1)}{(T_p s + 1)} \cdot M_1. \tag{10}$$

After taking inverse Laplace transform of equation 10 and some approximations, we get

$$M_R = \frac{k_c T_o}{T_p} \cdot M_1. \tag{11}$$

Again the DC motor with the electrical circuit is defined as

$$\tau_2 = \frac{k_2}{T_{21}s + T_{20}} \cdot u_2. \tag{12}$$

The above equations (1-12) can be combined as state space form as follows:

$$\begin{aligned}
&\frac{d\alpha_v}{dt} = \dot{\alpha}_v \\
&\frac{d\dot{\alpha}_v}{dt} = \frac{a_1}{I_1}\tau_1^2 + \frac{b_1}{I_1}\tau_1 - \frac{M_g}{I_1}\sin\alpha_v - \frac{B_{1a_v}}{I_1}\dot{\alpha}_v \\
&+ \frac{0.0326}{2I_1}\sin(2\alpha_v)\,\dot{c} - \frac{k_{\text{ov}}}{I_1}a_1\cos(\alpha_v)\,\dot{\alpha}_h {\tau_1}^2 \\
&- \frac{k_{av}}{I_1}b_1\cos(\alpha_v)\,\dot{\alpha}_h\tau_1 + w_1 \\
&\frac{d\alpha_h}{dt} = \dot{\alpha}_h + w_2 \\
&\frac{d\dot{\alpha_h}}{dt} = \frac{a_2}{I_2}{\tau_2}^2 + \frac{b_2}{I_2}\tau_2 - \frac{B_{1\alpha_h}}{I_2}\dot{\alpha}_h - \frac{k_c a_1}{I_2}1.75{\tau_1}^2 - \frac{1.75}{I_2}k_c b_1\tau_1 \\
&\frac{d\tau_1}{dt} = -\frac{T_{10}}{T_{11}}\tau_1 + \frac{k_1}{T_{11}}u_1 \\
&\frac{d\tau_2}{dt} = -\frac{T_{20}}{T_{21}}\tau_2 + \frac{k_2}{T_{21}}u_2,
\end{aligned} \tag{13}$$

where the terms w_1 and w_2 which symbolize the wind effects on the system are multi sin waves. We define the state variables as $x_1 = \alpha_v$ is the pitch angle, $x_3 = \alpha_h$ is the yaw angle, $x_2 = \Omega_v$ is the pitch angular velocity in the vertical plane, $x_4 = \Omega_h$ is the yaw angular velocity in the horizontal plane, $x_5 = \tau_1$ is the momentum of main motor and $x_6 = \tau_2$ is the momentum of tail motor. The complete state equations of the TRMS can be derived as (Saroj et al. (2013))

$$\begin{aligned}
\dot{x_1} &= x_2 \\
\dot{x_2} &= \frac{a_1}{I_1}{x_5}^2 + \frac{b_1}{I_1}x_5 - \frac{M_g}{I_1}\sin x_1 - \frac{B_{1\alpha_v}}{I_1}x_2 \\
&+ \frac{0.0326}{2I_1}\sin(2x_2)\,x + w_1 - \frac{k_{\sigma_1}}{I_1}a_1\cos(x_1)\,x_4{x_5}^2 \\
&- \frac{k_{q_1}}{I_1}b_1\cos(x_1)\,x_4x_5 \\
\dot{x_3} &= x_4 \\
\dot{x_4} &= \frac{a_2}{I_2}{x_6}^2 + \frac{b_2}{T_2}x_6 - \frac{B_{1\alpha_h}}{I_2}x_4 - \frac{k_c a_1}{T_2}1.75{x_5}^2 \\
&- \frac{1.75}{T_2}k_c b_1 x_5 + w_2 \\
\dot{x_5} &= -\frac{T_{10}}{T_1}x_5 + \frac{k_1}{T_{11}}u_1 \\
\dot{x_6} &= -\frac{T_{22}}{T_{21}}x_6 + \frac{k_2}{T_{21}}u_2.
\end{aligned} \tag{14}$$

This approach accounts for external disturbances arising from wind gusts, with the multi-sin signal chosen as the wind gust source. Dynamic of the wind gust, consist of summation of distinct sinusoidal excitation with bias, which is based on Dryden model, is defined as follows Waslander and Wang (2009)

$$w = w_i 0 + \sum_{k=1}^{n} a_{i,k} sin(\omega_{i,k}t + q_{i,k}), \quad i = 1, 2, 3$$

The given expression represents a combination of n sinusoidal components that define a wind gust model, where each sinusoid is characterized by its amplitude ($a_{i,k}$), frequency ($\omega_{i,k}$), and phase shift ($q_{i,k}$). The variable di0 denotes the static part of the wind gust. It's important to note that the disturbance $d_i(t)$ and its derivatives are continuous and bounded. system parametrs description and values can be found in table1:

Table 1. Discription of the TRMS model parameters.

Parameter and Description	Value(Unit)
Moment of inertia of vertical rotor(I_1)	0.068(kgm^2)
Moment of inertia of horizontal rotor(I_2)	0.02(kgm^2)
Static characteristic(a_1)	0.0135 (N/A)
Static characteristic(a_2)	0.02 (m)
Static characteristic(b_1)	0.0294 (m)
Static characteristic(b_2)	0.09 (m)
Gravity momentum(M_g)	0.32 (Nm)
Friction momentum function($B_{1\alpha_v}$)	0.006 (N-m-s/rad)
Friction momentum function($B_{1\alpha_h}$)	0.01 (N-m-s/rad)
Gyroscopic momentum parameter(K_{gy})	.0155 (s/rad)
Main rotor gain(k_1)	1.1 (N/A)
Tail rotor gain(k_2)	0.8 (N/A)
Main rotor denominator(T_10)	1 (N/A)
Main rotor denominator(T_11)	1.1 (N/A)
Main rotor denominator(T_20)	1 (N/A)
Main rotor denominator(T_21)	1 (N/A)
Cross reaction momentum parameter(T_p)	2 (N/A)
Cross reaction momentum parameter(T_0)	3.5 (N/A)
Cross reaction momentum gai(k_c)	-0.2 (N/A)

3. DATA-DRIVEN MODEL-FREE ADAPTIVE MULTIVARIABLE CONTROL METHOD

The Dynamic Linearization MFAC method effectively manages nonlinear systems like the TRMS. Three MFAC variants (FFDL, PFDL, and CFDL) are applied and compared for their tracking capabilities. FFDL provides a strong foundation, while PFDL and CFDL offer specialized solutions based on FFDL. MFAC's core principle, dynamic linearization, estimates a time-varying linear representation of an unknown nonlinear plant using past inputs, outputs, and current outputs. This approach better captures the plant's dynamic features by incorporating additional degrees of freedom. Underlying the design of dynamic linearization-based MFAC schemes is the general controllability assumption Hou and Jin (2013):

Assumption 1. The plant must exhibit output controllability, allowing for the discovery of control signal sequences that minimize the tracking error within a finite time for any feasible reference input.

Consider the following nonlinear process model to present the general MIMO MFAC approach:

$$y(k+1) = f(y(k), ..., y(k-n_y), u(k), ..., u(k-n_u)), \tag{15}$$

where, $u(k) \in R$ is the input, and $y(k) \in R$ is the output at time instant k, and it is assumed that the positive integers n_y and n_u, as well as the vector-valued function f, are unknown in the given MIMO system. The FFDL method is a generalized dynamic linearization form of the DDMFAC, as depicted in Figure 1.

Assumption 2. The partial derivatives of the function $f(\cdot)$ in 15 are continuous with respect to all variables in the system, ensuring smoothness and well-behaved dynamics throughout the entire problem domain.

Assumption 3. The nonlinear plant described by Equation 15 adheres to the generalized Lipschitz condition, which is

$|y(k_1+1)-y(k_2+1)| \leq b||H_{Ly,L_u}(k_1)-H_{Ly,L_u}(k_2)||$ for any $H_{Ly,L_u} \neq H_{Ly,L_u}, k_1, k_2 \geq 0$, and b is a positive constant.

Consider the nonlinear plant given by 15. Then, for any selected $0 \leq L_y \leq n_y$ and $0 \leq L_u \leq n_u$, provided that $||\Delta H_{L_y,L_u}(k)|| \neq 0$, there exists a time-varying vector $\phi_{f,L_y,L_u}(k) \in \mathrm{R}^{L_y+L_u}$, called the pseudo-gradiant (PG) such that 15 can be presented in the following linear time-varying multivariable FFDL data model:

$$\Delta y(k+1) = \phi^T_{f,L_y,L_u}(k)\Delta H_{L_y,L_u}(k) \tag{16}$$

where $\phi_{f,L_y,L_u}(t) = [\phi_1(t), \cdots, \phi_{L_y}(t), \cdots, \phi_{L_y+L_u}(t)]^T$ is bounded for all t, and $\Delta y(k+1) = y(k+1) - y(k)$, and $\Delta H_{L_y,L_u}(k) = [\Delta y(k), \cdots, \Delta y(k-L_y+1), \Delta u(k), \cdots, \Delta u(k-L_u+1)]^T$. $[k-L_u+1, k]$ and $[k-L_y+1, k]$ are plant input moving window and plant output moving window, respectively, and L_u and L_y are positive integers representing the plant pseudo orders or the control input and output LLC, respectively. Moreover, for each $k < 0$ we have $H_{Ly,L_u}(k) = 0_{Ly,L_u}(k)$.

The control performance index function is expressed as:

$$J(u(k)) = [(y_d(k+1)-y(k+1))^2+\lambda(u(k)-u(k-1))^2] \tag{17}$$

where $y_d(k+1)$ represents the desired input signal, and $\lambda > 0$ denotes the weighting factor. By incorporating equation 16 into equation 17 and minimising 17 $\frac{\partial J(u(k))}{\partial u(k)} = 0$, we get:

$$\begin{aligned} u(k) = u(k-1) + \frac{\rho_{L_{y+1}}\phi_{L_{y+1}}(k)}{\lambda + \phi_{L_{y+1}}(k)^2}[y_d(k+1) - y(k)] - \\ \frac{\phi_{L_{y+1}} \sum_i^{L_y} \rho_i \phi_i(k) \Delta y(k-i+1)}{\lambda + \phi_{L_{y+1}}(k)^2} - \\ \frac{\phi_{L_{y+1}} \sum_{i=L_{y+2}}^{L_y+L_u} \rho_i \phi_i(k) \Delta u(k+L_y-i+1)}{\lambda + \phi_{L_{y+1}}(k)^2} \end{aligned} \tag{18}$$

where $\rho_i \in (0,1], i = 1, 2, , L_y + L_u$ makes the $u(k)$ more general, as ρ is an additional step size factor. For general nonlinear systems, the $u(k)$ in 18 cannot be directly applied with respect to the time-varying and uncertain pseudo-gradient PG $\phi_{L_y,L_u}(k)$. Therefore, to address this issue, an online parameter estimation method is required to estimate $\phi_{L_y,L_u}(k)$. We define the estimation criterion function for PPD $\phi_{L_y,L_u}(k)$ as follows:

$$\begin{aligned} J(\phi_{f,L_y,L_u}(k)) = |y(k) - y(k-1) - \phi^T_{f,L_y,L_u}(k)\Delta H_{L_y,L_u}(k-1)|^2 \\ \mu||\phi_{f,L_y,L_u}(k) - \hat{\phi}_{f,L_y,L_u}(k-1)||^2 \end{aligned} \tag{19}$$

The weighting factor μ is a positive constant that balances error and regularization terms in the estimation criterion function. Minimizing 19 with the matrix inversion lemma, we obtain the following estimate for $\phi_{f,L_y,L_u}(k)$:

$$\begin{aligned} \hat{\phi}_{f,L_y,L_u}(k) = \hat{\phi}_{f,L_y,L_u}(k-1) + \frac{\eta \Delta H_{L_y,L_u}(k-1)}{\mu + ||\Delta H_{L_y,L_u}(k-1)||^2} \\ \times [\Delta y(k) - \hat{\phi}^T_{f,L_y,L_u}(k-1)\Delta H_{L_y,L_u}(k-1)] \end{aligned} \tag{20}$$

where the step factor η , within the range of (0,2], is used to provide a degree of freedom to control the impact of the correcting term.

The MFAC based on PFDL and CFDL algorithms follows a similar principle to the FFDL method. When L_y is 0 and L_u is 1, the FFDL-based MFAC method can be transformed into the CFDL-based MFAC method, and when L_y is 0 and L_u is a positive integer, the FFDL-based MFAC method can be transformed into the PFDL-based MFAC method. In this specific context, we are dealing with a known system, and its characteristics are well-understood. Given this knowledge, it becomes intuitive to select pseudo orders that align with their exact values in order to optimize the performance of the dynamically linearized model. This approach, generally helps maintain a balance between

computational complexity and model accuracy for systems with varying degrees of complexity.

4. SIMULATION AND RESULTS

This section presents a thorough simulation-based analysis to validate the effectiveness of the three DDMFAC methods: CFDL, PFDL, and FFDL. The main goal is to showcase the performance of these controllers when applied to an unknown system utilizing only I-O data, without needing a known system model, and to evaluate their ability to track and control the nonlinear TRMS system under varying conditions. The results demonstrate the effectiveness of the MFAC method and highlight the unique strengths of its variants in managing complex, time-varying nonlinear systems.

Figure 1 illustrates the system's performance under different wind conditions. When $w_1 = w_2 = 0$, the system experiences a wind-free situation with no wind disturbances. Additionally, the figure depicts the system's behavior under windy conditions, utilizing the Dryden-based wind gust model. This model includes a static component (bias) equal to 1 and a dynamic component represented by $0.01sin(0.001t + \pi/10) + 0.01sin(0.02t) + 0.02sin(0.01t)$. This dynamic component is a combination of various sinusoidal excitations to simulate wind disturbances. The performance and tracking capability of the proposed controllers are illustrated in Figure 2, which displays the system outputs (yaw and pitch angles) alongside the desired signals.

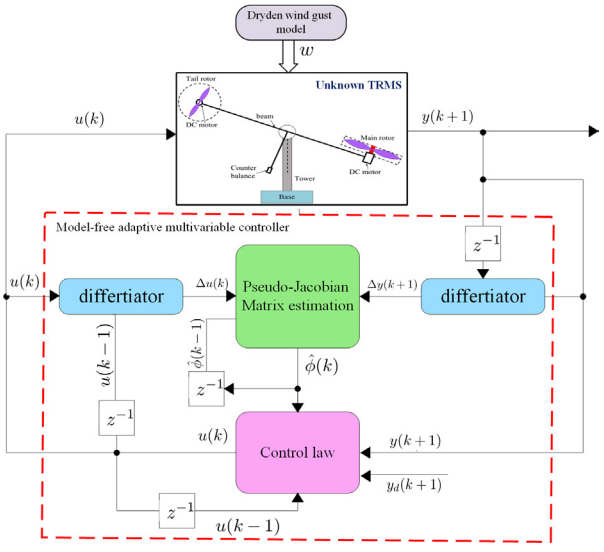

Fig. 1. Comparision of different DDMFAC schemes in wind-free stituation.

Figure 2 illustrates the performance of the three methods, highlighting the significant control effort exerted by CFDL to track the reference signal. While CFDL maintained the system within a bounded region, it exhibited notable chattering, especially in the y_2 output. In contrast, PFDL and FFDL demonstrated superior tracking capabilities, with FFDL outperforming PFDL in both y_1 and y_2 outputs. The smoother control response and enhanced accuracy of FFDL underscore its potential for effective reference tracking in complex systems.

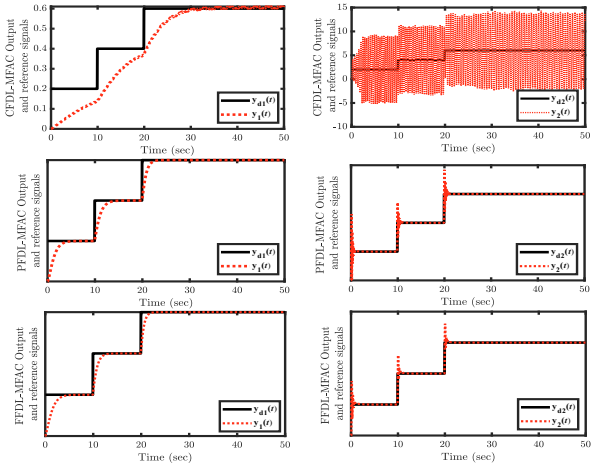

Fig. 2. Comparision of different DDMFA schemes in windy stituation.

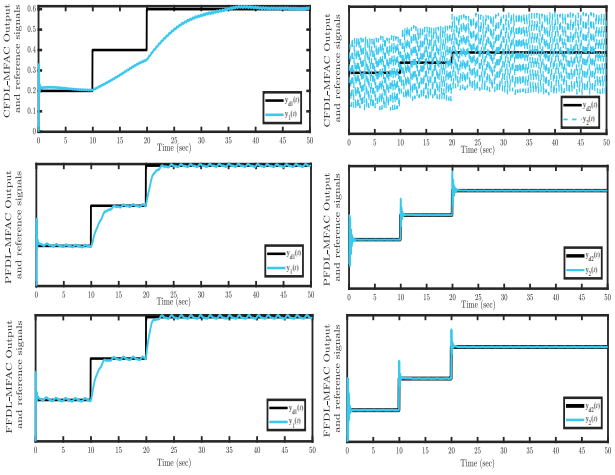

Fig. 3. The outputs of different DDMFA controllers under the windy situation.

To further validate the robustness of the developed control algorithm, we employed a multi-sinusoidal signal that closely mimics the behavior of a fan (wind) placed in close proximity to the TRMS. To further assess the robustness of the developed control algorithm, we introduced a multi-sinusoidal signal simulating wind gusts from a nearby fan, effectively creating a more realistic environment for the Twin Rotor MIMO System (TRMS). Figure 3 effectively showcases the performance and tracking capabilities of the proposed controllers in response to these wind gust conditions. The system outputs (yaw and pitch angles) are plotted alongside the reference signals, enabling a clear evaluation of each controller's effectiveness under such circumstances. From the graphical representation, it

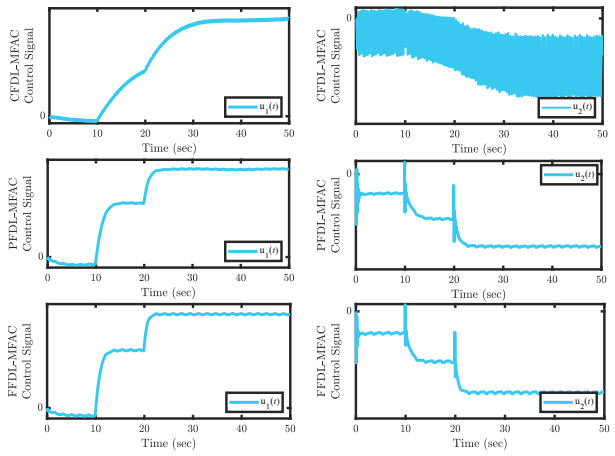

Fig. 4. DDMFAC in windy situation.

becomes evident that the CFDL method, while successfully maintaining the system's outputs within a bounded region around the desired reference signal, exhibits notable chattering. In contrast, both PFDL and FFDL methods demonstrate commendable performance under wind gust conditions. Notably, the FFDL method exhibits superior tracking capabilities and a smoother control response when compared to the other two methods, highlighting its potential for effective control in real-world scenarios involving uncertain system dynamics and external disturbances.

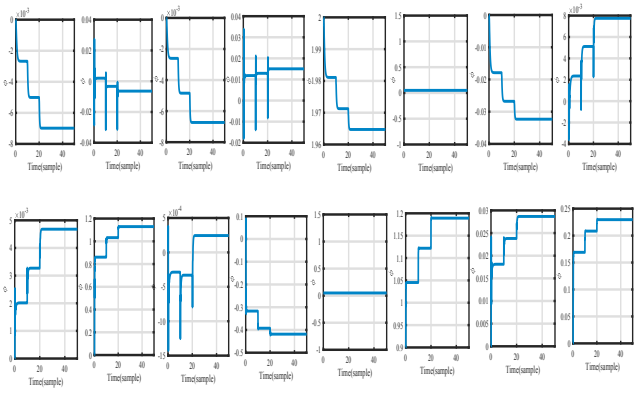

Fig. 5. PPD estimation of FFDL approach in wind-free situation.

The pseudo-gradient (PPD) estimates for the FFDL scheme are presented in Figures 5 and 6, depicting both wind-free and windy conditions. The results confirm that all elements of the time-varying FFDL-MFAC matrix remain bounded in both scenarios. Similar boundedness was observed for CFDL and PFDL, though these results are omitted due to space constraints.

The pseudo-gradient estimates for the FFDL scheme are presented in Figures 5 and 6, depicting both wind-free and windy conditions. The results confirm that all elements of the time-varying FFDL-MFAC matrix

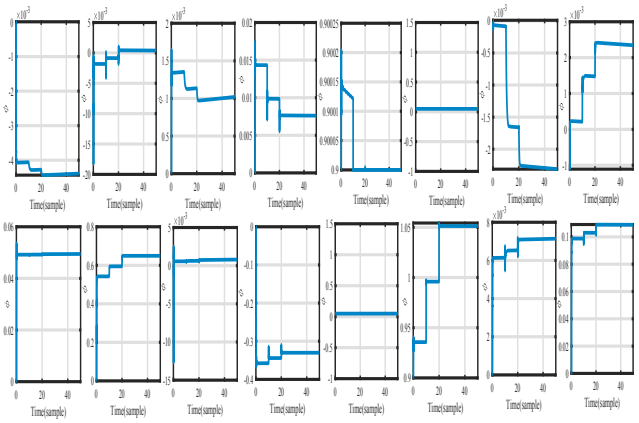

Fig. 6. PPD estimation of FFDL approach in windy situation.

Table 2. Error Analysis for Outputs y_1 and y_2 against windy and non-windy Conditions.

algorithm	output	MSE	RMSE
CFDL + wind	y_1	0.0069	0.0831
CFDL + wind	y_2	29.1310	5.3973
PFDL+wind	y_1	0.0012	0.0345
PFDL+wind	y_2	0.0236	0.1536
FFDL+wind	y_1	8.2950e-04	0.0288
FFDL+wind	y_2	0.0137	0.1170
CFDL	y_1	0.0093	0.0966
CFDL	y_2	29.3259	5.4153
PFDL	y_1	0.0014	0.0377
PFDL	y_2	0.0253	0.1591
FFDL	y_1	0.0012	0.0343
FFDL	y_2	0.0164	0.1282

remain bounded in both scenarios. Similar boundedness was observed for CFDL and PFDL, though these results are omitted due to space constraints.

The comparative analysis of the MFAC methods revealed that the FFDL method outperformed the other techniques in both the presence and absence of wind disturbances. Across various scenarios, the FFDL method consistently demonstrated superior control performance and tracking ability, setting it apart as the most effective algorithm among those evaluated.

To provide further quantitative support for the observed performance differences among the MFAC methods, we present a table featuring error metrics. In this case, we include the Mean Squared Error (MSE) and Root Mean Squared Error (RMSE) values for each method in both the presence and absence of wind disturbances. The MSE calculates the average squared error between the actual and desired output signals, while the RMSE is the square root of the MSE, representing the standard deviation of the residuals.

The error analysis in Table 2 highlights the superior performance of the FFDL method over PFDL and CFDL in both wind-free and windy scenarios. For example, FFDL achieved an RMSE of 0.0288 for y_1 and y_2 in windy conditions, which is 65 percent

lower than CFDL's RMSE of 0.0831. Similarly, for y_1 and y_2, FFDL's RMSE of 0.1170 was significantly lower than CFDL's 5.3973. These results demonstrate FFDL's enhanced tracking accuracy and robustness against external disturbances.

Future studies may explore incorporating additional information, such as disturbance input and output signals, into the system to further enhance the tracking capabilities and overall control performance of the DDMFAC methods. This could potentially lead to more effective adaptive control strategies that are even more resilient against external disturbances and uncertain system dynamics.

5. CONCLUSION

In this study, three DDMFAC methods—CFDL, PFDL, & FFDL—were evaluated for controlling a MIMO TRMS. The goal was to achieve precise beam tracking & accurate positioning in 2 DOF, even under wind disturbances. The results showed that FFDL outperformed CFDL & PFDL in both wind-free & windy conditions. FFDL demonstrated superior tracking accuracy, smoother control responses, & lower error metrics (MSE & RMSE) for pitch & yaw angles. PFDL also performed well but with slightly higher errors, while CFDL exhibited significant chattering & higher tracking errors.

The study highlights the potential of data-driven, model-free approaches for controlling complex nonlinear systems like the TRMS. By using only I-O data, these methods eliminate the need for precise system modeling, making them practical for real-world applications. The boundedness of the PPD estimates further validated the stability & robustness of the proposed control algorithms.

Future work could explore integrating additional disturbance info into the control framework to enhance tracking performance & robustness. Extending these methods to other complex systems or testing them in real-time experimental setups could provide further insights into their practical applicability. Overall, this study contributes to adaptive control strategies, demonstrating the effectiveness of FFDL-based DDMFAC in managing challenging control problems with external disturbances.

REFERENCES

CANKURT, R.T. (2018). Modeling and control of a twin rotor system.

Godbolt, B., Vitzilaios, N.I., and Lynch, A.F. (2013). Experimental validation of a helicopter autopilot design using model-based pid control. *Journal of Intelligent & Robotic Systems*, 70, 385–399.

Hou, Z. and Jin, S. (2013). *Model free adaptive control*. CRC press Boca Raton, FL, USA:.

Juang, J.G., Huang, M.T., and Liu, W.K. (2008a). Pid control using presearched genetic algorithms for a mimo system. *IEEE Transactions on Systems, Man, and Cybernetics, Part C (Applications and Reviews)*, 38(5), 716–727.

Juang, J.G., Lin, R.W., and Liu, W.K. (2008b). Comparison of classical control and intelligent control for a mimo system. *Applied Mathematics and computation*, 205(2), 778–791.

Rahideh, A., Bajodah, A.H., and Shaheed, M.H. (2012). Real time adaptive nonlinear model inversion control of a twin rotor mimo system using neural networks. *Engineering Applications of Artificial Intelligence*, 25(6), 1289–1297.

Rahideh, A., Shaheed, M.H., and Bajodah, A.H. (2007). Adaptive nonlinear model inversion control of a twin rotor system using artificial intelligence. In *2007 IEEE International Conference on Control Applications*, 898–903. IEEE.

Roman, R.C., Precup, R.E., and Radac, M.B. (2017). Model-free fuzzy control of twin rotor aerodynamic systems. In *2017 25th Mediterranean conference on control and automation (MED)*, 559–564. IEEE.

Roman, R.C., Radac, M.B., Precup, R.E., and Petriu, E.M. (2015). Data-driven optimal model-free control of twin rotor aerodynamic systems. In *2015 IEEE International Conference on Industrial Technology (ICIT)*, 161–166. IEEE.

Sandino, L.A., Bejar, M., and Ollero, A. (2013). A survey on methods for elaborated modeling of the mechanics of a small-size helicopter. analysis and comparison. *Journal of Intelligent & Robotic Systems*, 72, 219–238.

Saroj, D.K., Kar, I., and Pandey, V.K. (2013). Sliding mode controller design for twin rotor mimo system with a nonlinear state observer. In *2013 International Mutli-Conference on Automation, Computing, Communication, Control and Compressed Sensing (iMac4s)*, 668–673. IEEE.

Tao, C.W., Taur, J.S., and Chen, Y. (2010). Design of a parallel distributed fuzzy lqr controller for the twin rotor multi-input multi-output system. *Fuzzy Sets and Systems*, 161(15), 2081–2103.

Waslander, S. and Wang, C. (2009). Wind disturbance estimation and rejection for quadrotor position control. In *AIAA Infotech@ Aerospace conference and AIAA unmanned... Unlimited conference*, 1983.

Wen, P. and Lu, T.W. (2008). Decoupling control of a twin rotor mimo system using robust deadbeat control technique. *IET Control theory & applications*, 2(11), 999–1007.